Journal of Russian Laser Research, Volume 17, Number 1, 1996

MODELING AND EXPERIMENTAL STUDY OF 780-808-nm AlGaAs/GaAs INJECTION LASERS WITH ELECTRON SUPERLATTICE BARRIERS

V. V. Bezotosny,[1] Guan Rong Guo,[2] Guan Xin Guo,[2] P. V. Karga,[1] Zhang Qi Lin,[2] and Zhang Zheng De[2]

[1] *P. N. Lebedev Physical Institute, Russian Academy of Sciences, Leninsky Pr. 53, Moscow 117924, Russia*
[2] *HSRI, Hebei, Shijiazhuang, P.R. China*

Abstract

Electron superlattice barriers (ESBs) were used in AlGaAs/GaAs injection lasers to improve the electron confinement of the active layer by Bragg reflection of electron waves. The design of a separate-confinement heterostructure (SCH) laser with ESBs operating at 780–808 nm was optimized. Conventional SCH and SCH–ESB were prepared by low-pressure MOCVD epitaxy. Oxide stripe lasers with stripe widths of 100 and 200 μm were prepared. The threshold current density of 0.3 kA/cm^2 and the characteristic temperature constant T_0 = 220 K were measured at a wavelength of 808 nm for SCH–ESB lasers with an active-layer thickness of 40 nm and a resonator length of 0.4–0.5 mm. For conventional SCH lasers with the same geometry, a threshold current density of 0.42 kA/cm^2 and T_0 = 160 K were obtained. Experimental results on the low-temperature photoluminescence characterizing ESB regions are presented and are compared with the calculated miniband energy spectrum of the superlattice structure. The leakage currents for ordinary SCH and SCH–ESB lasers were analyzed. Experimental verification of a reduction in the leakage current for SCH–ESB lasers was obtained.

1. Introduction

It is well known that the threshold current of conventional double heterostructure (DH) lasers is strongly temperature-dependent. In a narrow temperature interval, this dependence can be adequately expressed as

$$J_{\text{th}}(T) = J_0 \exp \frac{T}{T_0} ,$$

where the characteristic temperature constant T_0 describes the temperature sensitvity. For AlGaAs/GaAs DH lasers at room temperature, T_0 equals 160–180 K. However, the number of carriers capable of overcoming a heterojunction barrier by thermal excitation increases with increasing temperature of the active layer. This tends to increase the threshold current and strengthen its temperature dependence, and consequently to decrease T_0. Such a temperature dependence of the threshold current is the principal cause of the limitation of the maximum output power in cw and quasi-cw operation. This problem is more pronounced in high-output-power lasers and arrays used for pumping solid-state lasers and laser heterostructures based on ternary and quarternary materials, namely, GaInP/AlInP, InGaAsP/InP, and AlGaInP/GaAs, which have lower T_0 values in comparison with the AlGaAs/GaAs system. Improvement of the temperature dependence is the main problem in obtaining high output power, efficiency, and reliability in high-output-power operation and improving the radiation characteristics of ternary and quarternary laser materials.

Original article submitted in English August 26, 1995.

1071-2836/96/1701-0085$15.00

One of the approaches to solving this problem is the use of superlattice barriers for electrons. Electron superlattice barriers (ESBs) were proposed in [1] for the improvement of electron confinement in heterostructures. It is also anticipated [2] that heterojunction barrier enhancement by electron wave reflection from appropriately designed superlattice structures will improve the radiation characteristics of visible injection lasers. Lasers based on GaInP/AlInP heterostructures for the spectral range of 660–680 nm and a laser based on an AlGaInP/GaAs heterostructure at 600 nm exibit carrier leakage at room and elevated temperatures, which makes it difficult to achieve a low threshold current density and efficient cw operation. That is why experimental verification of the ESB idea was performed at first for shortwave (660–680 nm) GaInP/AlInP heterojunction lasers.

According to [3], a drastic improvement in lasing characteristics was observed. The threshold current density was as low as 840 A/cm^2 and the characteristic temperature constant T_0 was as high as 167 K. The same parameters for lasers without ESBs were 2000 A/cm^2 and 110 K, respectively. However, the results of [3] gave no direct evidence of a "pure" ESB effect on the lasing characteristics because the current density and its temperature dependence were measured and compared for conventional laser structures without ESBs and structures with ESBs and superlattice confinement layers (SCL). Results on lasers with ESBs but without SCL were not presented. At the same time, the decrease in threshold current density, the main effect observed in [3], was obtained due to SCL, whereas the improvement in the temperature dependence was attributed to the use of ESBs. For lasers with SCL, the temperature constant was even smaller (101 K) than for a conventional laser. It is difficult to explain these results just on the basis of additional electron confinement. It is likely that the results of [3] had an influence on the authors of [4], where short-period superlattice (SPS) confinement layers were applied to an InGaAs/GaAs/AlGaAs structure. As a result, no difference in threshold current density between conventional and SPS lasers was observed, whereas the improvement in the temperature dependence was drastic. To the best of our knowledge, T_0 = 240 K for SPS lasers, and T_0 = 90 K for conventional lasers were obtained.

We believe that our work is the first direct confirmation of the effect of ESBs on the lasing characteristics of AlGaAs/GaAs heterostructures. The SCH type of AlGaAs/GaAs heterostructure was chosen as the most interesting object for investigation of new physical phenomena. This structure is the most technologically advanced. It has no limitations caused by lattice-matching problems and reproducibility of parameters. The present work was also stimulated by practical application of high-output-power laser arrays and modules operating at 808 nm for pumping solid-state lasers, because an improvement in laser structure homogeneity and an increase in the characteristic temperature constant T_0 are the key problems in this field. One more reason for the application of ESBs to heterostructures operating at 780–808 nm is deterioration of the laser parameters with decreasing wavelength.

The available literature data on the wavelength dependence of the threshold current density of broad-area lasers with a resonator length of 450–500 μm were analyzed in [5]. For conventional DH lasers, as well as for quantum well lasers, the tendency toward an increasing threshold current density with decreasing wavelength below 830 nm is obvious. The best results reported by different groups on DH and quantum well lasers at 800 nm are in the range of 0.5–0.8 kA/cm^2. At the same time, the tendency toward a sharper increase in threshold current density is of significance for quantum well lasers. Thus, improvement of the parameters of an AlGaAs/GaAs heterostructure used for lasers at 810 nm and shorter wavelengths is an important practical problem.

2. Calculation of ESB Parameters

ESB parameters were calculated on the basis of the envelope function approximation [6], in which electron waves in an AlGaAs/GaAs superlattice obey the dispersion relationship

$$\begin{aligned} \cos(KD) &= \cos(k_w d_w)\cos(k_b d_b) - \frac{1}{2}\left(x + \frac{1}{x}\right)\sin(k_w d_w)\sin(k_b d_b), \\ x &= \frac{k_w m_b}{k_b m_w}, \end{aligned} \tag{1}$$

where d_w and d_b, k_w and k_b, and m_w and m_b are, respectively, the thicknesses of the well and the barrier layers, the wave vectors, and the effective masses in them,

$$D = d_w + d_b$$

is the thickness of a single cell in an ESB, and K is the Bloch wave vector. Relationship (1) determines the band structure of an AlGaAs/GaAs superlattice. Real parts of K correspond to allowed bands of the superlattice, and imaginary parts K_i correspond to band gaps.

We studied the dependence of the reflection coefficient of electron waves from an ESB on the electron energy. The analysis was performed on the basis of an analytical expression [7] that in the case of an AlGaAs/GaAs superlattice with N periods has the form

$$\begin{aligned} |r_N|^2 &= \frac{|C|^2}{|C|^2 + \left(\dfrac{\sin KD}{\sin NKD}\right)^2}, \\ C &= \frac{1}{2}i\left(x - \frac{1}{x}\right)\sin k_b d_b, \end{aligned} \tag{2}$$

where i is the unit imaginary number. The value of K is found from (1). In the superlattice band gaps, we have

$$KD = m\pi + iK_i D,$$

i.e., KD is a complex number. Then the expression for the reflection coefficient becomes

$$|r_N|^2 = \frac{|C|^2}{|C|^2 + \left(\dfrac{\sinh K_i D}{\sinh NK_i D}\right)^2}. \tag{3}$$

If N is large, the second term in the denominator of expression (3) tends to zero and the reflection coefficient r_N for the superlattice band gaps is close to unity. A considerable portion of the electrons with energies corresponding to superlattice band gaps is therefore reflected from an ESB.

The ESB parameters, namely, the layer thickness, the composition, and the number of periods, were chosen on the basis of expressions (1) and (3). As noted above, relationship (1) can be used to determine the band structure of an ESB. A suitable selection of ESB parameters makes it possible to place the second band gap of an ESB above the potential barrier formed by the barrier layer. This is shown in Fig. 1, where the shaded regions indicate the positions of the first and second band gaps formed in an ESB. If the number of periods N is sufficiently large, electrons with higher energies are also reflected and this results in an effective increase in the barrier height for electrons by an amount equal to the second band gap of the ESB. In other

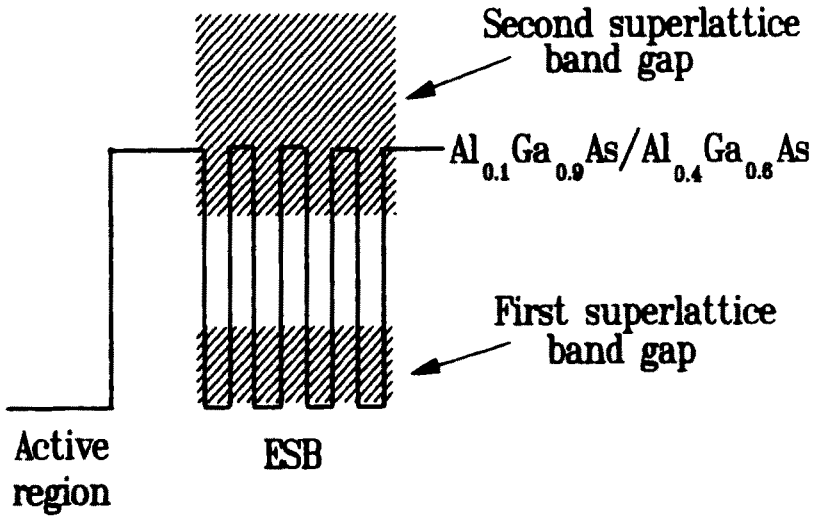

Fig. 1. Energy diagram of an ESB. The shaded regions are energy band gaps in superlattices.

words, the ESB configuration is bound to conform to the Bragg slit placed above the potential barrier. With this occurring, the superlattice reflects carriers that have the possibility of overcoming the barrier by thermal exitation.

The ESB parameters were chosen taking into account the technological capabilities of the apparatus used to grow the heterostructures and the condition that the energy of the laser photons should be smaller than the energy of the transitions between the first allowed electron and hole superlattice bands in order to prevent absorption of these photons in ESB regions.

The introduction of ESB regions in a SCH laser can give good results only in the case of precise control of the superlattice parameters: material quality, aluminium content, and layer thickness. It is of practical importance to evaluate the necessary accuracy of these parameters for the most interesting case where the aluminium content is about 0.1 in the active layer and 0.4 in the barrier layer. The minizone structure was calculated versus the period of ESBs for electrons and heavy and light holes (Fig. 2). On the basis of these calculations, we evaluated the parameters of ESBs.

3. Sample Preparation

Laser heterostructures (Fig. 3) were grown by low-pressure MOCVD:

The starting materials for the growth process were trimethylgallium (TMG), trimethylaluminium (TMA), and AsH_3. H_2Se at 100 ppm was used as the Se source for n–type doping, and liquid CCl_4 was used as the carbon source for p–type doping.

The total hydrogen flow was 6 liter/min, and the pressure was 45 mbar.

The ratio of V-group elements to III-group elements was 60.

The growth temperature was 700° C.

The growth temperature of the p^+–GaAs contact layer was 520° C.

Waveguide layers, ESB regions, barrier layers, and the active layer were grown without doping.

The electron concentration in the GaAs buffer layer and the n–type $Al_{0.6}Ga_{0.4}As$ layer was about $5 \cdot 10^{17}$ cm

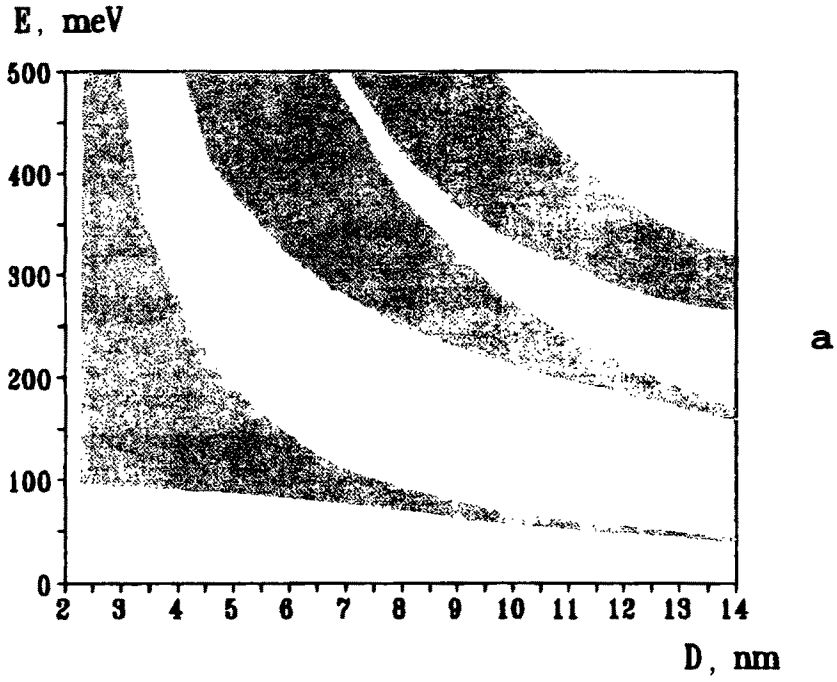
E, meV
500
400
300
200
100
0
2 3 4 5 6 7 8 9 10 11 12 13 14
D, nm

a

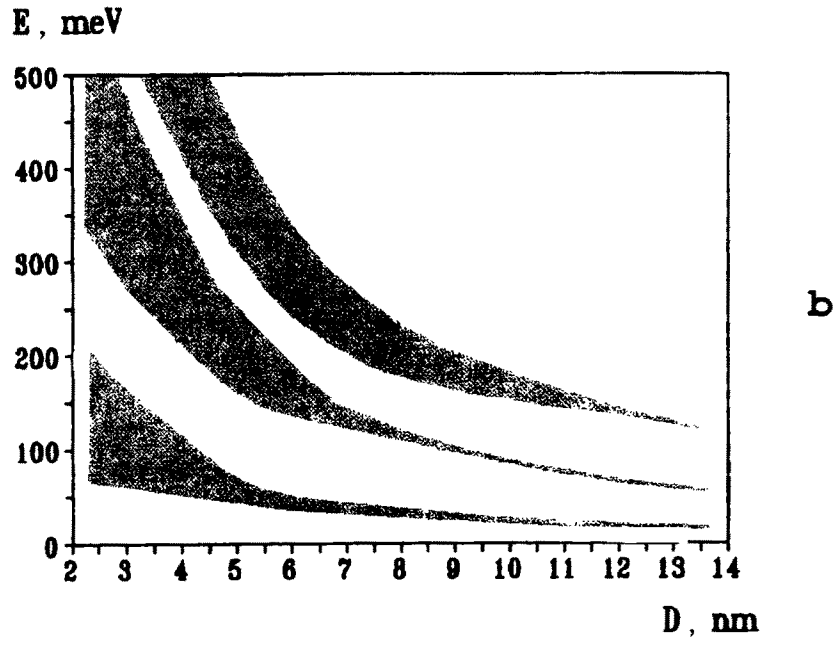
E, meV
500
400
300
200
100
0
2 3 4 5 6 7 8 9 10 11 12 13 14
D, nm

b

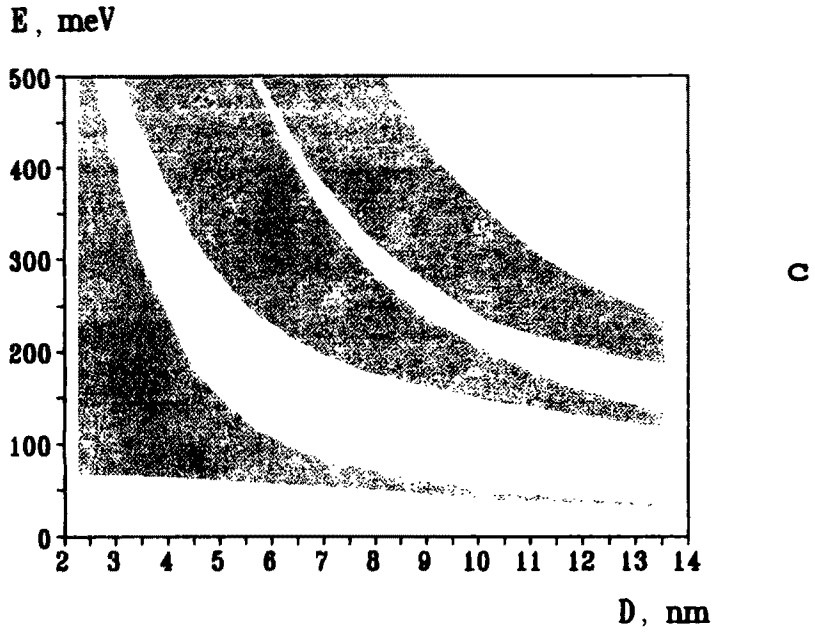

Fig. 2. Band structure of an $Al_{0.4}Ga_{0.6}As/Al_{0.1}Ga_{0.9}As$ superlattice versus the period D for electrons (a), heavy holes (b), and light holes (c). $d_w = d_b$, $k_\perp = 0$. The allowed energy bands are shaded.

The hole concentration was $6 \cdot 10^{18}$ cm^{-3} in the p–$Al_{0.6}Ga_{0.4}As$ emitter, and $1.5 \cdot 10^{19}$ cm^{-3} in the p^+–GaAs contact layer.

The GaAs substrate was inclined at an angle of 2–3° with respect to the (100) plane toward the ⟨110⟩ direction.

For comparison, the conventional SCH structure was grown.

The active-layer thickness of 40 nm and the total waveguide thickness of 280 nm were the same for all structures, including the conventional SCH structure.

Both $Al_{0.6}Ga_{0.4}As$ emitters were 1.4 μm thick, and the p^+–GaAs contact layer was 0.3–0.5 μm thick. This heterostructure design with a bulk 40-nm active layer was used in order to prevent the influence of quantum well effects.

Stripe geometry lasers were prepared with Si_3N_4 dielectric insulation 100–nm thick formed by plasma deposition. Channels 100 and 200 μm wide were formed in the Si_3N_4 film by photolithography and plasma etching.

Both sides of the structure were metallized and alloyed. An additional Au film was plated electrochemically.

Before bonding to a heat sink, laser diodes were tested by measurement of the V–I characteristics and the threshold current in the pulsed-operation regime.

Laser diodes were mounted on Au-plated copper heat sinks with In solder head-up to prevent mirror deterioration and to be sure that the optical output was free. The upper electrode was connected to the laser diode by a gold wire using the ultrasonic thermocompression method.

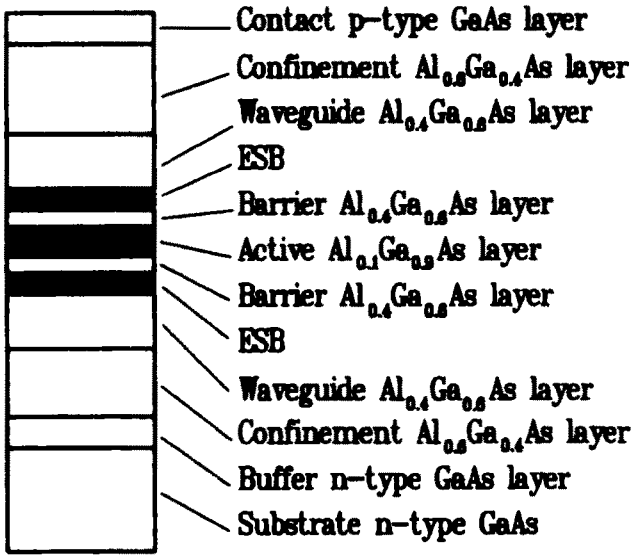

Fig. 3. Schematic diagram showing an AlGaAs/GaAs heterostructure with electron superlattice barriers (ESBs).

4. Spectral Characteristics

The presence of ESBs in laser structures was evidenced by low-temperature photoluminescence (PL) measurements. Samples under investigation were placed in a helium cryostat. The temperature was stabilized close to 18 K. The PL was excited by an Ar laser and analyzed by a computer-controlled spectrometer. The diameter of the excited area of a sample was 0.5 mm. The PL spectrum of a conventional SCH sample is shown in Fig. 4a. A shortwave peak at 675 nm in PL spectra of SCH–ESB samples appears in addition to peaks of other layers (Fig. 4b). The peak at 775 nm corresponds to luminescence of the active layer, at 830 nm – to the buffer layer, and at 870 nm – to the p^+–GaAs contact layer. The shortest-wave peak at 620 nm is relatively weak because it corresponds to $Al_{0.4}Ga_{0.6}As$ waveguide layers whose composition is close to that of the indirect gap semiconductor.

The main distinction between PL spectra of different structures was observed in the spectral range of 650–720 nm, corresponding to the superlattice region; not only was spectral broadening of the superlattice PL peak clearly observed, but double-peaked spectra were also recorded. Such broadening, according to [8], characterizes the quality and uniformity of structure layers. Double-peaked spectral shapes are a result of island formation on the boundary of superlattice layers. According to calculations, the spectral shift between these two peaks corresponding to different layer thicknesses is rather large even in the case of one-monolayer steps on the boundaries when the total thickness of the layers is small, as in our case with 8–10 monolayers. Therefore, the presence of an ESB region and the measurement of PL spectra from the superlattice area of the structure can be used as a very sensitive indicator of the interface structural quality of an epitaxial structure. The example of a uniform superlattice region characterized by a single-peaked spectrum is presented in Fig. 4b; the double-peaked spectrum from the ESB region of another structure is shown in Fig. 4c.

Information about the uniformity of the samples was obtained by measuring PL spectra at different points on the heterostructure surface. A characteristic feature of these measurements is the same structure of spectral lines at different points. Only small variations in the position of luminescence peaks were observed. More interesting information was obtained at different temperatures and excitation levels. At high excitation

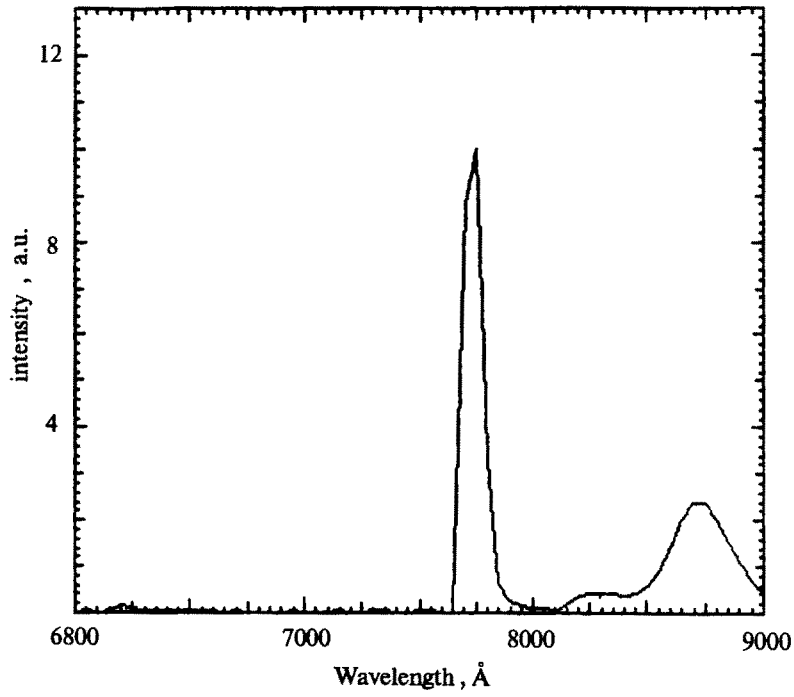
12
8
4
intensity , a.u.
6800
7000
8000
9000
Wavelength , Å

a

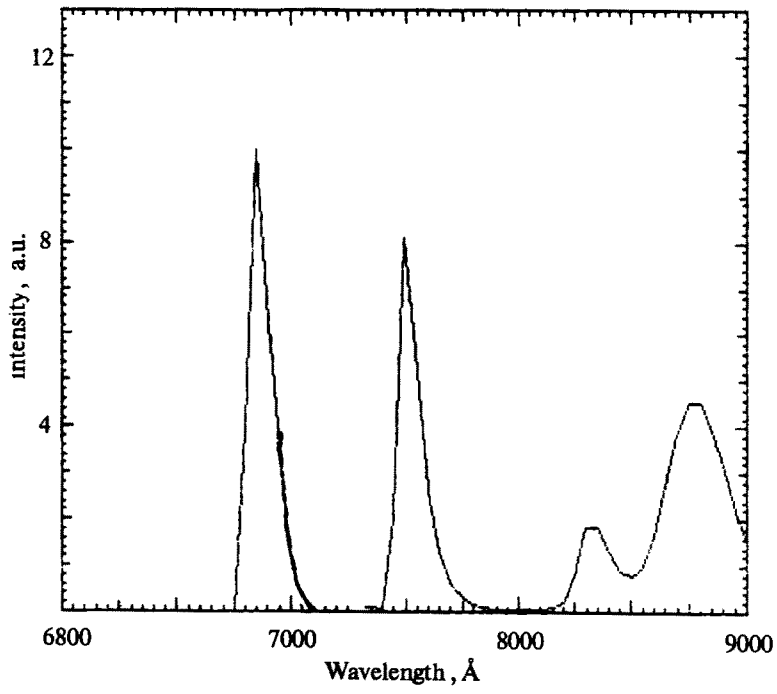
12
8
4
intensity , a.u.
6800
7000
8000
9000
Wavelength , Å

b

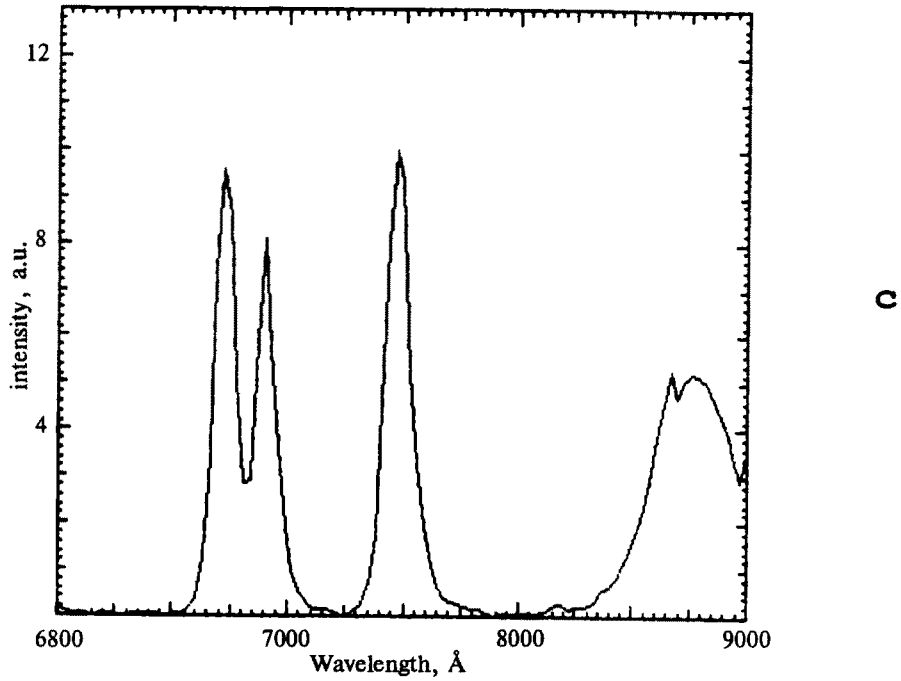

Fig. 4. Photoluminescence spectra of the conventional SCH (a), SCH–ESB with one peak from the ESB region (b), and SCH–ESB with two peaks from the ESB region (c).

levels, double-peaked spectra of ESB regions become quadruple-peaked. This behavior is attributable to transitions between the first electronic minizone (e1) and the first minizones of heavy (hh1) and light (lh1) holes. At high excitation levels, the probability of radiative transitions that involve higher-energy lh1 zones is of the same order of magnitude as the probability of e1–hh1 transitions. A temperature increase enhances the rate of nonradiative recombination and decreases the intensity of e1–lh1 transitions relative to the intensity of e1–hh1 transitions at the same excitation level.

At room temperature, the PL signal from ESB regions was at the noise level and the active-layer line was formed completely by e1–hh1 transitions. This result is in accordance with [9], where double-peaked PL spectra from superlattice samples were described as bound- and free-exciton transitions. Bound excitons are associated with islands (steps) at superlattice interfaces and free excitons – with superlattice regions of uniform thickness. The relative intensity of these two peaks is different at low and high temperatures and at different excitation levels. The relative intensity of the shortwave peak of the superlattice doublet is higher at 150 K, whereas at 77 K the superlattice spectrum is characterized by four peaks and the intensity of the shortwave peaks is lower than the intensity of the longwave peaks. We propose the following model of the phenomenon. The relative growth of a shortwave peak is attributable to the enhancement of free-exciton transitions at elevated temperatures caused by the fact that the thermal energy becomes close to the exciton binding energy. At 77 K, on the other hand, four peaks are resolved at a high excitation level. This can be described by e1–lh1 and e1–hh1 transitions. At the same temperature of 77 K and a low excitation level (Fig. 4c), the superlattice region has a double-peaked spectrum.

The energy of the e1–hh1 and e1–lh1 transitions was calculated versus the superlattice period. The minizone positions for electrons and light and heavy holes presented in Fig. 2 for $Al_{0.1}Ga_{0.9}As/Al_{0.4}Ga_{0.6}As$ structures with superlattice periods from 2 to 14 nm were compared with experimental data. It is possible

to evaluate from this comparison the actual period of an ESB structure using experimental data on the position of PL spectral peaks. The variation in ESB layer thickness calculated from the positions of ESB spectral peaks for the laser structures used in our experiments was 1–2 monolayers. This gives evidence of the conditions that were adequate for high-quality epitaxial growth of the laser structure and, moreover, evidence of the basic limitations of thickness control for wells and barriers in the ESB structure.

According to the calculated properties of ESBs, such variations in thickness produce a difference in the effective potential barrier enhancement for electrons in the range of 115–210 meV for structures with a one-monolayer thickness variation and in the range of 70–210 meV for structures with a two-monolayer thickness variation. In actuality, structures with single- and double-peaked PL spectra of ESBs were obtained under the same growth conditons. Therefore, the variation in thickness of different structures and the variation in electron confinement efficiency were at the limits of the MOCVD apparatus used for structure growth.

5. Threshold Current

We observed a correlation between the threshold current density and the variation in ESB layer thickness. The lowest threshold current density of 0.3 kA/cm^2 and at the same time the highest characteristic temperature constant T_0 were obtained for lasers produced from a structure with just one narrow PL peak observed from the ESB section. It is clear that the quality of the interfaces governs the laser cavity loss; at the same time, the efficiency of carrier confinement due to ESBs affects the leakage current and determines the threshold current density of a laser.

The carrier leakage current was calculated using results for double-heterostructure lasers [10] modified for the SCH–ESB. The procedure involved determination of the minority-carrier densities in the cladding layer at the barrier layer interfaces and subsequent determination of the minority diffusion currents. Let us perform approximate calculations neglecting the electron transport through the ESB regions and assuming that the carrier concentration is equal to that in the bulk material. The influence of ESBs on leakage currents is taken into account by means of an effective barrier height that equals the sum of the potential barrier height due to the band gap discontinuity between the active and cladding layers and the second superlattice band gap.

Let us consider electrons in the Γ valley in the p–cladding layer. At the interface, their density is given by the expressions

$$\begin{aligned} n_p^\gamma &= N_c^\gamma F_{1/2}\left(\frac{F_n - V_{\text{eff}}}{kT}\right), \\ N_c^\gamma &= 2\left(\frac{2\pi m_n^\gamma kT}{h^2}\right)^{3/2}, \\ F_{1/2}(y) &= \frac{2}{\pi^{1/2}}\int\limits_0^\infty \frac{x^{1/2}dx}{1+\exp(x-y)}, \end{aligned} \tag{4}$$

where F_n is the quasi-Fermi level of the conduction band with respect to the band edge and

$$V_{\text{eff}} = V + E_{\text{gap}}^{\text{supl}}$$

is the effective barrier height, which equals the sum of the cladding barrier height and the second superlattice band gap. The Fermi integral can be approximated reasonably well by the expanson

$$F_{1/2}(y) \simeq e^y - \frac{e^{2y}}{2^{3/2}} + \cdots + (-1)^{m+1}\frac{e^{my}}{m^{3/2}}.$$

A satisfactory result can be obtained for $-\infty < y < -2.1$.

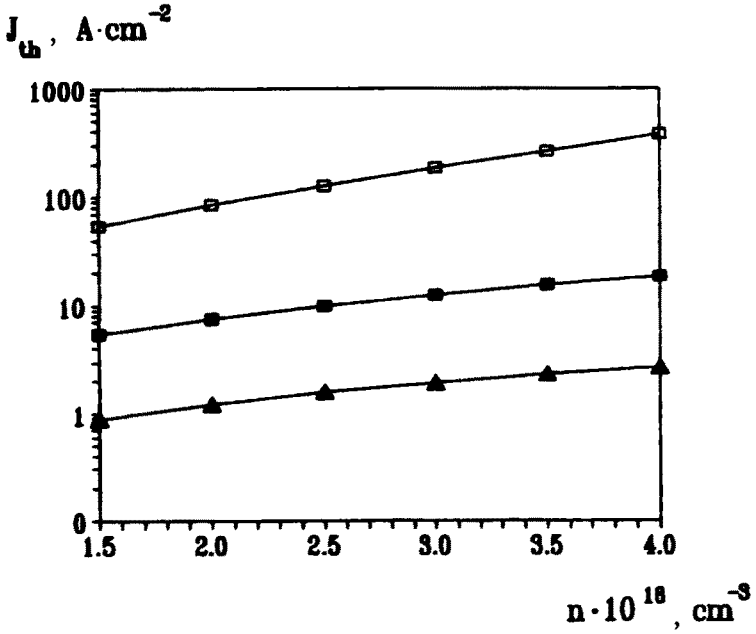

Fig. 5. Total leakage current as a function of the concentration of injected electrons and holes for conventional SCH lasers (□) and SCH–ESB lasers with barrier and layer thickness of 2.83 nm (■) and 2.26 nm (▲).

Then we solved the equation for diffusion of minority carriers in the p–cladding layer using the boundary conditons $n_p = n_p^\gamma$ at the interface of the barrier and active layers and $n_p = 0$ at the p–side ohmic contact, a distance x_p from the interface. As a result, the minority carriers give the following density of electron leakage current from the Γ valley:

$$J_n^{\text{diff}} = \frac{qD_n n_p^\gamma}{L_n \tanh(x_p/L_n)}, \tag{5}$$

where D_n is the electron diffusion coefficient and L_n is the electron diffusion length. The calculations were made for $D_n = 50\ \text{cm}^2 \cdot \text{s}^{-1}$, $x_p = 1.2\ \mu\text{m}$, and $L_n = 1\ \mu\text{m}$.

Expressons similar to (4) and (5) were used to calculate the leakage currents from the Γ valence band corresponding to heavy and light holes. The additional contribution made to the total leakage current by drift transport of minority carriers, which can be significant when the electric field in the cladding layers is strong, is neglected. The calculated results are shown in Table 1 and Fig. 5.

TABLE 1. Total leakage current as a function of the concentration of injected electrons and holes for conventional SCH lasers and SCH–ESB lasers with a barrier and layer thickness of 2.83 and 2.26 nm.

	J_{leak}, A·cm^{-2}		
n, cm^{-3}	SCH	ESB (2.83 nm)	ESB (2.26 nm)
$1.5 \cdot 10^{18}$	54.02	5.46	0.89
$2.0 \cdot 10^{18}$	84.65	7.55	1.23
$2.5 \cdot 10^{18}$	126.59	9.83	1.57
$3.0 \cdot 10^{18}$	184.63	12.36	1.93
$3.5 \cdot 10^{18}$	265.30	15.22	2.31
$4.0 \cdot 10^{18}$	377.39	18.51	2.71

The evidence for leakage currents in the 780–810-nm structures was obtained from spectral measurements of spontaneous emission. Figure 6 shows spectral curves of cw spontaneous emission measured at room temperature for lasers with current injection below threshold. Curves (a) and (b) are measured for the conventional SCH laser and the SCH–ESB laser, respectively. Longwave peaks are clearly observed in both samples. The emission close to 915 nm corresponds to the highly doped p^+–contact layer. The intensity of the 915-nm peak is much higher for the laser without ESBs.

Two possible mechanisms of formation of longwave peaks in 780–810-nm AlGaAs/GaAs structures were considered: carrier leakage and optical pumping by spontaneous emission. In actuality, the effect of optical pumping is much weaker than that of current leakage. This is indicated experimentally by the absence of the longwave peak at 870 nm corresponding to the n–GaAs buffer layer. The luminescence intensity of the n–GaAs buffer layer doped to a level of $5 \cdot 10^{17}$ cm^{-3} and being optically pumped by spontaneous emission from the $Al_{0.1}Ga_{0.9}As$ active layer must be even higher than the luminescence intensity of the p^+–GaAs contact layer because the conditions of optical pumping are the same for both layers. This suggests that the longwave peak in spontaneous emission is evidence of current leakage from the active layer.

Other evidence of the fact that the mechanism of formation of the longwave peak is associated with carrier leakage from the active layer and not with optical pumping was obtained from measurement of the relative areas of the peaks at 810 and 915 nm at elevated temperatures. At high temperature, the intensity of spontaneous emission at 810 nm decreases due to nonradiative recombination and carrier leakage. Optical pumping of the contact and buffer layers also decreases with increasing temperature in line with the 810 nm peak intensity. But carrier leakage causes an increase in the relative area of the 915-nm peak. This behavior was observed experimentally. Thus, it seems likely that the leakage current in 810-nm lasers and especially in 780-nm lasers is one of the main restrictions on their radiation characteristics.

It is impossible to increase the heterojunction barrier height by increasing the aluminum concentration in the cladding layers. When the Al content exceeds 0.42, the nondirect-gap $Al_xGa_{1-x}As$ cannot provide better carrier confinement. As a result, $Al_xGa_{1-x}As$ layers with $x > 0.4$ may be useful for SCH heterostructures

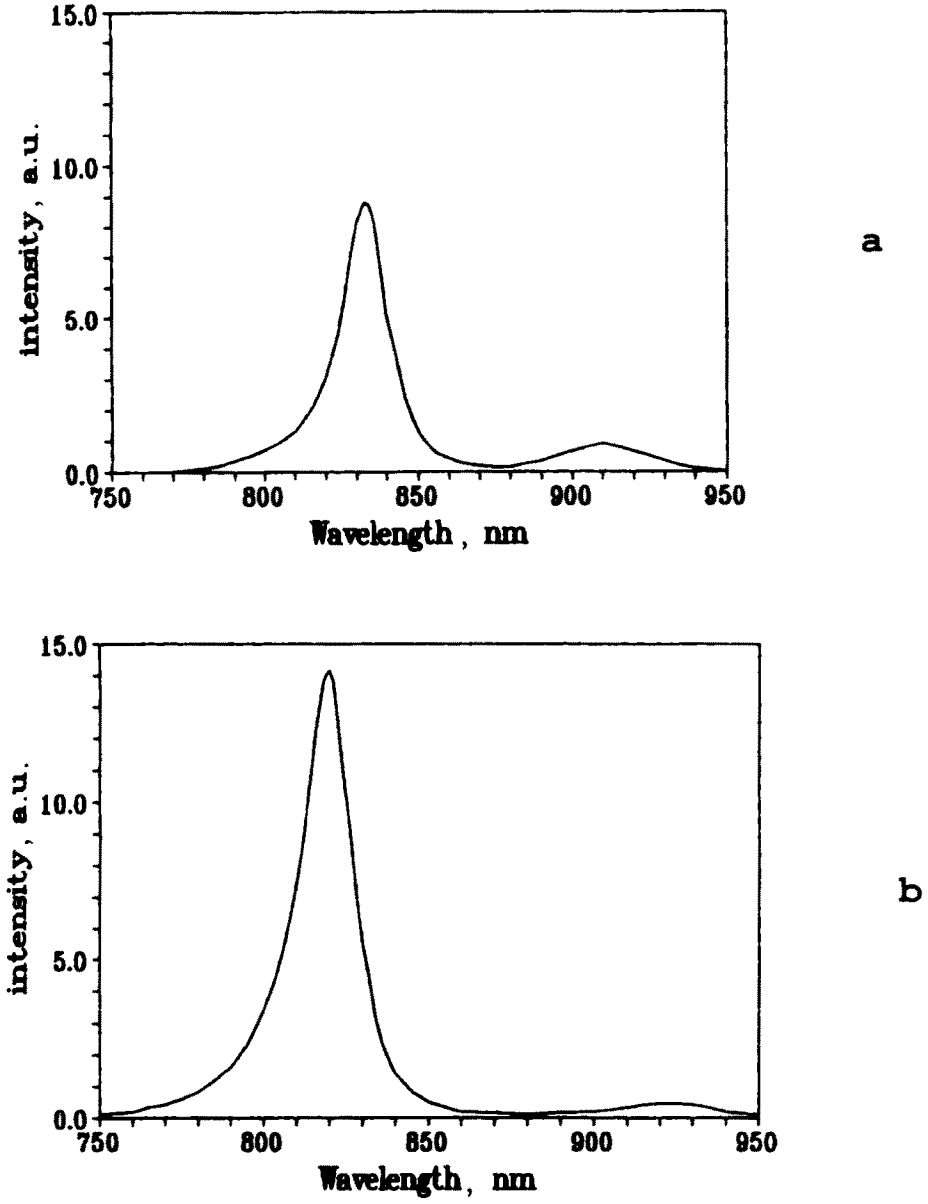

Fig. 6. Spontaneous emission spectra for the conventional SCH laser (a) and the SCH–ESB laser (b).

operating at 780–810 nm only for improving the optical confinement. Direct evidence of leakage current reduction due to ESBs was obtained by measuring the relative areas of longwave spontaneous emission for conventional SCH lasers and SCH–ESB lasers. The power of the longwave peak in SCH–ESB lasers was approximately three times lower. This result is in good agreement with calculations by expression (4). The reduction in leakage current in SCH–ESB lasers due to improvement of carrier confinement can explain the decrease in threshold current and the increase in characteristic temperature constant T_0.

The best results on threshold current density and temperature characteristics were obtained for the lasers with ESBs shown in Fig. 3. The structure was characterized by single-peaked PL from the ESB region.

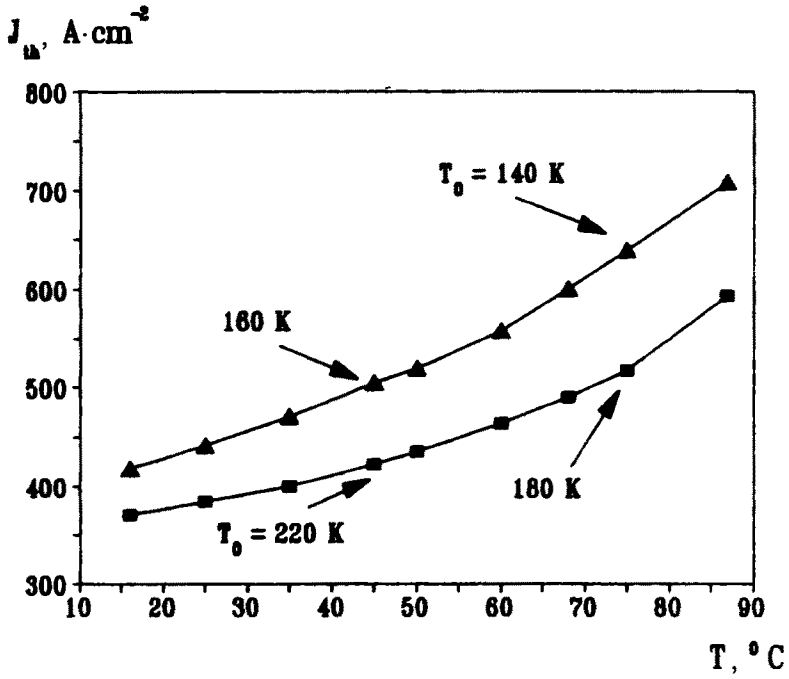

Fig. 7. Temperature dependence of the threshold current density of stripe lasers with conventional geometry (▲) and lasers with ESBs (■).

The superlattice consisted of 7 periods formed of $Al_{0.1}Ga_{0.9}As/Al_{0.4}Ga_{0.6}As$ layers with equal thicknesses of 2.26 nm for wells and barriers.

Laser diodes for a study of the temperature dependence of the threshold current were selected using the following fast-test procedure:

The threshold current was measured at different pulse widths from 5 to 150 μs. As the pulse width approached 100 μs, the changes in the threshold current for samples with optimized ESBs were very small. Conventional SCH lasers exibited comparably large changes in the threshold current.

The SCH and SCH–ESB laser diodes selected by this technique were mounted on heat sinks. After testing the V–I and light–current characteristics, the selected samples were used for measurements of the temperature dependence of the threshold current. Typical temperature dependences of the threshold current for SCH and SCH–ESB lasers are shown in Fig. 7. The threshold current densities of SCH and SCH–ESB lasers at 16° C were equal to 0.42 kA/cm^2 and 0.31 kA/cm^2, respectively.

The threshold current density of SCH–ESB and conventional SCH lasers ranged from 0.3 to 0.4 and from 0.42 to 0.55 kA/cm^2, respectively.

Such a large difference in threshold current density between SCH and SCH–ESB lasers was not predicted theoretically earlier. This difference is caused by the fact that additional electron confinement influences only electrons with above-barrier energy. The number of such electrons is determined by the tail of the Fermi–Dirac distribution. The main effect of ESBs must become evident at high temperatures, when the number of high-energy electrons increases. We were surprised that the difference in threshold current density between SCH and SCH–ESB lasers with optimized geometry was measured to be 25–30%.

The threshold current density for SCH–ESB lasers with nonoptimal ESB parameters was the same as for conventional SCH lasers. This difference induced us to investigate the possibility of carrier leakage from the active layer at room and even at low temperatures. Temperature dependences of the threshold current were

measured for the SCH sample with the lowest threshold current density of 0.42 kA/cm^2 and a moderate-quality sample taken from optimized SCH–ESB lasers with a threshold current density of 0.36 kA/cm^2.

From Fig. 7 the characteristic temperature constant T_0 was found to be 220 K for the SCH–ESB laser and 160 K for the conventional SCH laser in the temperature range up to 50° C. At 75° C, the T_0 values are 180 K and 140 K, respectively. At temperatures below 35° C, the T_0 values for SCH–ESB lasers was up to 260 K.

The results obtained are encouraging because the waveguide structure of the samples under study was not optimum and the active-layer thickness was rather large, i.e., it did not correspond to the quantum well. To our knowledge, the value of 0.3 kA/cm^2 obtained for an active-layer thickness of 40 nm is the best result published for a wavelength of 810 nm and a resonator 450–500 μm long. It is our opinion that the results presented form a basis for further optimization of the laser structures.

References

1. K. Iga, H. Uenohara, and F. Koyama, *Electron. Lett.*, **22**, 1008 (1986).
2. T. Takagi, F. Koyama, and K. Iga, *Electron. Lett.*, **27**, 1081 (1991).
3. K. Kishino, A. Kikuchi, V. Kaneko, and I. Nomura, *Appl. Phys. Lett.*, **58**, 1822 (1991).
4. T. Hayakawa, K. Matsumoto, H. Horic, et al., *J. Appl. Phys.*, **74**, 5285 (1993).
5. P. Blood, *Heterostructures in Semiconductor Lasers, IEEE Materials and Devices*, Ser. 8, Exeter (1991), p. 262.
6. G. Bastard, *Phys. Rev. B*, **24**, 5693 (1981).
7. P. Yeh, A. Yariv, and G. Hong, *J. Opt. Soc. Am.*, **67**, 423 (1977).
8. N. Watanabe and Y. Mory, in: *Proc. II Intern. Conf. on Modulated Semiconductor Structures*, Kyoto (1985), p. 220.
9. E. S. Moskalenko, A. V. Akimov, and A. A. Kaplyanskii, in: *Abstracts of Papers Intern. Symp. Nanostructures: Physics and Technology* [in Russian], St. Petersburg (1995), p. 76.
10. H. C. Casey and M. B. Panish, *Heterostructure Lasers*, Academic Press, New York (1978), p. 248.